

Dynamics of a map with power-law tail

V. Botella-Soler[†], J.A. Oteo[‡] and J. Ros[†] §

[†]Departament de Física Teòrica and Instituto de Física Corpuscular, Universitat de València, 46100-Burjassot, València, Spain

[‡] Departament de Física Teòrica, Universitat de València, 46100-Burjassot, València, Spain

E-mail: vicente.botella@uv.es, oteo@uv.es, rosj@uv.es

Abstract. We analyze a one-dimensional piecewise continuous discrete model proposed originally in studies on population ecology. The map is composed of a linear part and a power-law decreasing piece, and has three parameters. The system presents both regular and chaotic behavior. We study numerically and, in part, analytically different bifurcation structures. Particularly interesting is the description of the abrupt transition order-to-chaos mediated by an attractor made of an infinite number of limit cycles with only a finite number of different periods. It is shown that the power-law piece in the map is at the origin of this type of bifurcation. The system exhibits interior crises and crisis-induced intermittency.

PACS numbers: 05.45.Pq, 05.45.Ac, 02.30.Oz

AMS classification scheme numbers: 37G35, 37M05, 74H99, 37D45

1. Introduction

Work on population ecology carried out in the 1970's certainly helped chaos to move center stage as a new interdisciplinary subject [1]. One-dimensional discrete-time models are technically among the simplest ones to consider and interpret. They provide an appropriate description of species with non-overlapping generations. The basic example for the evolution of a population density $X_n \in \mathbb{R}$ at generation n is the linear law $X_{n+1} = rX_n$. Here r represents the growth rate or fecundity, assumed constant. It is, however, too schematic allowing only extinction ($r < 1$), equilibrium ($r = 1$) or infinite growth ($r > 1$). It was soon recognized that more realistic models should be nonlinear:

$$X_{n+1} = X_n F(X_n). \quad (1)$$

Written in this form, F is the dimensionless non-constant fitness function of the population or per-capita growth rate. A sage choice for it should capture the essential features of the system. The crucial point is that once nonlinearity is let in, a huge variety of new phenomena may appear as is now universally recognized. Thus, discrete time population ecology is in close contact with discrete dynamical system theory. For instance, the choice [2, 3]

$$F(X_n) = r(X_n/K)^{-b}, \quad b > 0, \quad (2)$$

renders easy the numerical determination of the parameter values from experimental population data by a linear fit to $\log X_{n+1}$ versus $\log X_n$, which constitutes certainly a salient advantage. In (2) the presence of parameter K , the conventional carrying capacity, ensures the dimensionless character of F . A slight variant of it reads [3, 4]

$$F(X_n) = \begin{cases} r, & X_n \leq C \\ r(X_n/K)^{-b}, & X_n > C \end{cases} \quad (3)$$

where C is a threshold population density and the fitness parameter $b > 0$ is dimensionless.

For the purposes of the present paper we emphasize that these and similar models can also be used as mathematical instances of dynamical systems to illustrate different features when the ranges of parameters and time variable are enlarged beyond those realistic in population dynamics. In this spirit, we analyze here the one-dimensional discrete model associated with equation (3) which will be referred to as VGH (Varley-Gradwell-Hassell) [5]. In [6] it is briefly explained that the system is chaotic for $b > 2$ and regular for $b < 2$, pointing out that in the order-to-chaos transition no cascade of period doubling emerges. In the present paper we analyze numerically and analytically how such a transition takes place which, to the best of our knowledge, has not been studied in detail in the mathematics or ecology literature.

The system function is continuous for $C = K$ and discontinuous otherwise. Piecewise continuous maps are, by far, less analyzed than continuous ones in the literature. Also, we address our attention to the role of the threshold parameter C , to which no much attention seems to have been given.

The paper is organized as follows. In Section 2 we describe the features of the VGH map, present some traits of the associated dynamical system, and briefly introduce the pertinent equations to compute the Lyapunov exponent. In Section 3 the transition order-to-chaos is studied in detail. Some exact results are presented for $b = 2$ and an explanation for the observed bifurcation is propounded. In Section 4 the effect of varying C and r is analyzed. Finally, Section 5 contains our conclusions. For the sake of completeness, two technical Appendices are included. In particular, Appendix B contains a thorough analytical study of the VGH map in the critical case $b = 2$.

2. Description of the map and its dynamics

2.1. Alternative formulations

We write the VGH map, equation (3), in the form

$$x_{n+1} = f(x_n; b, c, r) \quad (4)$$

with

$$f(x; b, c, r) = \begin{cases} rx, & x \leq c \\ rx^{1-b}, & x > c \end{cases} \quad (5)$$

In going from (1) and (3) to (4) and (5) we have used the carrying capacity K as our natural unit to measure population densities and correspondingly introduced the dimensionless variable $x_n = X_n/K$, and parameter $c = C/K$.

The function f in (5) is defined in \mathbb{R}^4 although, being a population variable, we take $x \in [0, \infty)$. In the three dimensional parameter space (b, c, r) we consider only the region $b > 1$ to ensure decrease of f with increasing x ; $c, r > 0$ for compatibility with the range for x .

According to this map the population density in a given generation is a linear function of that in the previous one as far as it does not exceed a critical value c . For greater values the population follows a nonlinear power-law. Figure 1 illustrates the different possibilities and we expect, therefore, differences in the response of the system according to whether the value of c is below or above unity.

For some purposes, we have found it useful to express the VGH map in terms of the new variable z and the new parameter ξ

$$z \equiv 2 \log(x)/\log(r), \quad \xi \equiv 2 \log(c)/\log(r) \quad (6)$$

with $x \neq 0$ and $r > 1$. The numeric factor two in (6) has been introduced for convenience. The inverse transformation reads

$$x = r^{z/2}, \quad c = r^{\xi/2}. \quad (7)$$

This leads from (5) to

$$z_{n+1} = \begin{cases} z_n + 2, & z_n \leq \xi \\ (1-b)z_n + 2, & z_n > \xi \end{cases} \quad (8)$$

now with phase space $(-\infty, \infty)$. This representation of the map has just two effective parameters. From a mathematical point of view this transformed version is piecewise linear, whereas (5) defines a piecewise continuous nonlinear system. Linearization is a standard procedure in the study of dynamical systems. It usually follows from first order approximations. Here, however, the linearization is exact. In Appendix A we collect some results obtained from this version of the dynamical system. It is worth mentioning that dynamical systems of the same type can be found in applications in electronics, robotics and mechanical systems with impacts [7, 8].

2.2. VGH dynamical system

We present here some of the most apparent features of the dynamical system originated by the iteration of the VGH map.

First we can dispose of the case $r < 1$. $x = 0$ is then always an stable fixed point. When $c < r^{1/b}$ there is a second fixed point at $x = r^{1/b}$ which is stable if $1 < b < 2$ and which attracts any initial condition in the interval (c, x^*) with $x^* = (c/r)^{1/(1-b)}$. For $b = 2$, that interval consists of period-2 points, with the exception of the fixed point \sqrt{r} . Values $x \leq c$ and $x > x^*$ go to $x = 0$. Observe that here $r < 1$ does not necessarily imply extinction. This is due to the interplay between the different parameters.

For $r = 1$ any initial condition in $[0, c]$ remains fixed. If $c < 1$ then $x = 1$ is also fixed. It is stable for $1 < b < 2$ attracting any initial condition in the interval (c, x^*) with $x^* = c^{1/(1-b)}$. If $b = 2$, the interior points of that interval, except $x = 1$, are paired in 2-cycles. Points to the right of x^* are eventually fixed, reaching its limiting fixed value in two steps.

For $r > 1$, $x = 0$ is an unstable fixed point, independently of c . If $c < r^{1/b}$, also $x = r^{1/b}$ is fixed, although it is stable only for $1 < b < 2$.

In the rest of the paper we consider only $r > 1$ which, as we shall see, generates a much richer behavior.

2.3. Lyapunov exponent

The Lyapunov exponent is a measure of the rate at which two initially close trajectories move away. For the one-dimensional discrete map $x_{n+1} = f(x_n)$ the computation of the Lyapunov exponent λ admits an analytical formula (see for instance [9, 10, 11, 12])

$$\lambda = \lim_{n \rightarrow \infty} \left\{ \frac{1}{n} \sum_{k=0}^{n-1} \ln |f'(x_k)| \right\} \quad (9)$$

which, in the case (5), leads to

$$\lambda = \ln r + \lim_{n \rightarrow \infty} \left\{ \frac{1}{n} \sum_{k=0}^{n-1} [\ln |1 - b| - b \ln |x_k|] \theta(x_k - c) \right\}, \quad (10)$$

whereas (8) yields

$$\lambda = \ln |1 - b| \lim_{n \rightarrow \infty} \left\{ \frac{1}{n} \sum_{k=0}^{n-1} \theta(z_k - \xi) \right\}. \quad (11)$$

Both formulas are given in terms of Heaviside θ function which selects the iterations that visit $x_n > c$ or $z_n > \xi$ respectively.

The mathematical equivalence of the two expressions for λ in (10) and (11) yields the following result for the statistics of points $x_k > c$ in the attractor

$$\lim_{n \rightarrow \infty} \left[\frac{1}{n} \sum_{k=0}^{n-1} \ln(x_k) \theta(x_k - c) \right] = \frac{\ln r}{b} \quad (12)$$

which tells that the geometric mean of all the points $x_k > c$ in the trajectory equals the value $r^{1/b}$. A simpler version of (10) reads now

$$\lambda = \ln |1 - b| \lim_{n \rightarrow \infty} \left\{ \frac{1}{n} \sum_{k=0}^{n-1} \theta(x_k - c) \right\}. \quad (13)$$

Equation (9) makes use of the derivative f' which in the present case is not defined at $x = c$ or $z = \xi$. As it is an isolated point, it does not amount any numerical difficulty.

In practice, one has to take care of discarding transients in order to allow the orbit to enter the attractor. In particular, transients are very long for chaotic trajectories when $b \approx 2$. Besides, it is convenient to average λ over a number of initial seeds.

The interpretation of the Lyapunov exponent in this system is particularly straightforward: λ is ruled by the proportion of exterior points in the trajectories, namely those with $x_n > c$ or $z_n > \xi$.

Since the summation in (10) and (11) is over a large enough number of points on the trajectory, numerical accuracy is a relevant issue. To this end, and following the analysis in [13], we have used the multi-precision Fortran package MPFUN [14, 15] which allows one to efficiently compute with very high number of digits. We concluded that double precision gives here enough computational guaranties as regards (10) and (11). By contrast, it is not the case for the computation of trajectories of (8) with some integer values $b > 2$, an issue that we deal with in Section 4.5.

3. Dependence on b : order-to-chaos transition

As already stated in [6], the chaotic regime corresponds to $b > 2$, independently of the values of c and r , without stable regularity windows embedded. This is clear from the positive character of λ in (13) when $b > 2$.

In the limit $b \rightarrow 2^+$ the Lyapunov exponent becomes very small due to the term $\ln |1 - b|$, since the proportion of exterior points is finite. Following results on nonextensive thermodynamics it may be pertinent to wonder whether a power law n^γ is a more appropriate ansatz than the exponential $\exp(\lambda n)$ to measure the divergence of initially close trajectories [16, 17]. We have carried out a statistics of the largest

separations, in this limit, as a function of n and the results point out towards a clear exponential divergence.

The behaviour of the system with respect to b is illustrated by the bifurcation diagrams in Figure 2. The three panels correspond to $c = 1.2, 1, 0.8$, from top to bottom, respectively, with the fixed value $r = 2$. In Figure 3 we plot the bifurcation diagram for $c = 2.5$ and $r = 2$, as well as the Lyapunov exponent λ (upper panel). Notice the irregularities in the curve around the value $b = 2.2$ where the bifurcation diagram exhibits a number of band merging crises [12, 18].

The aforementioned sudden transition from a regular to a chaotic system, with no period doubling, is apparent. As the negative sign of the computed Lyapunov exponent witnesses, $b < 2$ means regular behavior: every initial seed ends up in a periodic orbit.

For fixed $b < 2$, the attractor consists of coexisting limit cycles. Its cardinal is a piecewise constant function of c . So, there exist some values $c = c_n$ ($n \geq 1$ integer) that punctuate the sequence of the number of points that make up the attractor. The cardinal is given by the heuristic formula $2(n+1)/[3 - (-1)^n]$, ($n \geq 1$), whose first few terms read

$$1, 3, 2, 5, 3, 7, 4, 9, 5, 11, 6, 13, 7, 15, 8, 17, 9, \dots \quad (14)$$

They can be interpreted as forming two intermingled sequences whose terms increase by one and two units respectively.

The diagram in Figure 4 gives a perspective of this situation for $b = 1.9$ and $r = 2$, as a function of c .

In the rest of this Section we focus our attention on the case $b = 2$ which separates the regular and chaotic regimes. We present both numerical and analytical results. The reader is referred to Appendix B for details.

3.1. Case $b = 2$.

For $b = 2$ and fixed $r > 1$ the orbit of an arbitrary initial condition $x_0 \in [0, \infty)$, is simple enough to be rigorously described. The behavior is varied and shows an interesting dependence on the parameter c . In particular this permits to appraise the effect of the discontinuity. As detailed below, the general characteristic in this case is that all the initial conditions are fixed, periodic or eventually periodic. There exist an infinity of coexisting limit cycles. Their periods are allowed to take only a restricted set of values, which depend on the initial condition and parameters value through very strict laws. We defer their detailed description to Appendix B. The reader can find there precise information about the transients length and exact account of the cycles. Here we report only the most salient features in terms of the variable x and threshold parameter c .

If $c \leq 1$, then the closed interval $[c, r/c]$ is invariant under the action of the map. Any interior point $x_0 \neq \sqrt{r}$ belongs to the 2-cycle $\{x_0, r/x_0\}$. $x_0 = \sqrt{r}$ is a fixed point. The extremes $x_0 = c$ and $x_0 = r/c$ as well as all the exterior points are eventually periodic, entering the invariant interval after a transient.

If $c > 1$, then the closed interval $[1/c, rc]$ is invariant under the action of the map. Every exterior point is eventually periodic. Interior points are periodic. For fixed c , the period of the cycles depends on x_0 but can take on only a restricted set of values. For instance, with $c = 2$ one finds a 3-cycle: $\{1/\sqrt{r}, \sqrt{r}, r\sqrt{r}\}$; a 4-cycle: $\{1/r, 1, r, r^2\}$; and the rest of the points in the interval accommodates in an infinity of 6-cycles. All these cycles are the limit cycles for the eventually periodic points. Notice that in this system the existence of period three does not imply chaos. This is not in conflict with the celebrated Li and Yorke theorem because the VGH map is defined by a discontinuous function.

The basins of attraction of such limit cycles are infinite intermingled sets of zero measure made of equidistant points in the z variable. The vertical segments located at $b = 2$ in Figures 2 and 3 comprise all the coexisting limit cycles. In numerical simulations such a vertical segment gets filled only if enough initial conditions are used in the construction of the bifurcation diagram.

3.2. An explanation of the observed bifurcation

Next we develop an heuristic explanation for the origin of the order-to-chaos bifurcation observed at $b = 2$. As is well known, period-2 points are fixed points of the second iterate $f^{[2]}$ of the map. In the cobweb plot of $f^{[2]}$ shown in Figure 5 the relevant element is the piece of $f^{[2]}$ which is co-linear with the bisectrix, because it conveys the existence of a continuous interval of fixed points. Leaving apart the fixed point of f , these points pair themselves to form the alluded period-2 orbits. By the cobweb construction the rest of the points eventually land in the piece on the bisectrix.

Whenever an infinite set of trajectories of period $n > 2$ is observed, with $b = 2$, it is because this value of the parameter forces $f^{[n]}$ to have one or more segments co-linear with the bisectrix too. The question is then: Which are the conditions for the map f to allow iterates $f^{[n]}$ to have pieces co-linear with the bisectrix?

Our answer is that the phenomenon may take place whenever the piecewise continuous map f has a piece defined by a power-law function. To buttress this answer let us write the general expression of a term of $f^{[n]}$ as

$$r^{p(b)}x^{(1-b)^m} \tag{15}$$

where $p(b)$ stands for a polynomial of b and $m \leq n \in \mathbb{N}$. Since $b > 1$, the conditions for (15) to be co-linear with the bisectrix are: even m , $b = 2$ and $p(2) = 0$.

To further illustrate this, let us focus on one part of the second iterate of (5), namely

$$f^{[2]}(x) = \begin{cases} \dots, & \dots \\ r^{2-b}x^{(1-b)^2}, & c < x < r/c, c < \sqrt{r} \end{cases} \tag{16}$$

where the dots stand for the three remaining terms and intervals in the definition of the second iterate. The explicit term of $f^{[2]}$ written down in (16) is co-linear with the bisectrix in the cobweb plot if and only if $b = 2$, as expected, provided $c < \sqrt{r}$. If

$c \geq \sqrt{r}$ the extremes of the interval collapse to a single point and that particular piece disappears in the second iterate.

In principle, several iterates can have co-linear terms simultaneously for the same value of c . This gives rise to coexisting cycles of different periods, a fact that is illustrated in the bifurcation diagram of Figure 6. There we have coded in color (gray tone) the periods of the trajectories, with fixed values $b = r = 2$. The representation is given in terms of $\{z, \xi\}$, which endows the plot with more symmetric structure. The intermingling of the colored rhombuses accounts for the coexistence of limit cycles with various periods. In addition, horizontal dashed (color) segments stand for cycles whose periods are indicated by circled numbers and have been taken from Table B1. Framed numbers indicate the corresponding period of orbits in rhombuses. As Figure 6 shows, for the parameter values considered, only two different iterates can have co-linear terms for the same value of ξ . Moreover, as ξ increases, more co-linear terms of successively higher iterates emerge whereas the co-linear terms of the previous iterates collapse and disappear (see Appendix B).

In other words, the presence of the rx^{1-b} power-law piece in the definition of the VGH model is at the origin of the bifurcation at $b = 2$. More generally, any one-dimensional map defined as a piecewise function, with a power-law piece in its definition, is a candidate to exhibit a bifurcation of the present type.

3.3. Case $b = 2$. When $x_0 = c$: Harter's boundaries

As is well known, for a continuous unimodal uniparametric map with its maximum at $x = x^*$, the plot of the successive iterates of the initial seed $x_0 = x^*$ versus the map parameter generates the so-called Harter boundaries [19, 20]. In the logistic map [1, 11, 21, 22], for instance, they correspond to the sharp cusps observed in the invariant density. These boundaries are, to some extent, the skeletal system of the bifurcation diagram where they are readily observed provided it is built up using color or grey tones. Harter lines cross at unstable equilibrium points and, in the case of the logistic map, the set of crossing points follows itself a reversed bifurcation cascade.

The VGH map is not differentiable at $x = c$, although it is still unimodal in the sense of being monotonically increasing for $x \leq c$ and decreasing for $x > c$. A similar study to the one described for the logistic map leads to interesting results. To be precise, Harter lines correspond to the color boundaries visible in Figures 2 and 3. They can be directly established from the form (5) of the map. It is nevertheless simpler to use instead (8) and the results gathered in Appendix A. For $b = 2$, the seed $x_0 = c$ ends up in a cycle whose period $P(r, c)$ depends on r and c . The expression for P and the cycle elements may be explicitly written down.

For $c < 1$ the 2-cycle $\{rc, 1/c\}$ is reached just after one iteration. For $c \geq 1$, $x = c$ is always a periodic point. Obviously $c = 1$ belongs to the 2-cycle $\{1, r\}$. When $c > 1$ there is a unique integer $M \in \mathbb{N}$ such that

$$c \in [r^{M/2}, r^{(M+1)/2}). \quad (17)$$

with

$$M = \left\lfloor 2 \frac{\log c}{\log r} \right\rfloor = \lfloor \xi \rfloor \quad (18)$$

in terms of the integer part or floor function. Then, for $c > 1$ we get two cases

$$P(r, c) = M + 2, \text{ if } c = r^{M/2} \quad (19)$$

$$P(r, c) = 2(M + 2), \text{ if } c \in (r^{M/2}, r^{(M+1)/2}) \quad (20)$$

The $2(M + 2)$ -points of the cycle for the case (20) read

$$\left\{ \frac{c}{r^M}, \frac{c}{r^{M-1}}, \dots, \frac{c}{r}, c, rc, \frac{1}{c}, \frac{r}{c}, \frac{r^2}{c}, \frac{r^{M+1}}{c} \right\} \quad (21)$$

which in turn, for $c = r^{M/2}$ (*i.e.*, case (19)) contract to the $(M + 2)$ -points cycle

$$\{r^{-M/2}, r^{-M/2+1}, \dots, r^{M/2-1}, r^{M/2}, r^{M/2+1}\} \quad (22)$$

It is interesting to observe that (21) can be obtained recurrently from $\{rc, 1/c\}$ by a simple procedure. In going from M to $M + 1$ two new elements are added to the cycle: the one in the leftmost position is obtained by dividing by r the first element in the previous cycle. The other, which goes at the rightmost position, is obtained by multiplying by r the last element of the previous cycle.

4. Dependence on c : Discontinuity location

The dependence of the system with respect to the parameter c with r fixed, or equivalently ξ , exhibits a large variety of features. We describe the system in the chaotic regime. First near the bifurcation point $b = 2$, and next for higher b .

4.1. Near $b = 2$

In Figure 7 we plot the bifurcation diagram as a function of c , computed with $b = 2.01$ and $r = 4$. For $c < 1$ the trajectories x_n wander in two relatively large chaotic bands in contrast with the extremely narrow ones for $c > 1$.

The upper panel in the figure gives the Lyapunov exponent. It is everywhere positive, as it must be for a chaotic regime. As a function of c , its value changes suddenly at every band merging crisis observed in the bifurcation diagram.

To study the diagram with further detail we present in Figures 8 – 10 magnifications of small areas in Figure 7.

The region with $c < 1$, near $b = 2$, has further interesting features. Thus, what in Figure 7 appears as two dense chaotic bands does have structure when minutely examined. Figure 8 shows this feature for the upper band. The grid structure in the bifurcation diagrams as a function of c (or ξ) fades as c decreases. The Lyapunov exponent in the upper panels exhibits jumps associated with chaotic bands merging crises.

For $c > 1$, the bifurcation diagram in Figure 8 exhibits further details after magnification. A zoom of the area indicated by the arrow is given in Figure 9 where a

sudden variation of the size of the attractor is apparent. This thin window is composed by twenty two chaotic narrow bands (only five in the zoom). Further, the crossing of Harter lines in Figure 11 punctuate the start and end of the shrunk chaotic bands. A unstable orbit exists inside the window, which is represented by the dashed lines in the Figure 11. Consequently, what we observe in Figure 9 as a shrinking and widening of the attractor corresponds, actually, to a pair of interior crisis [12, 18, 23]. Moreover, further interior crises of various smaller sizes appear inside the window itself in a, possibly, self-similar way. For instance, in the leftmost part of this bifurcation diagram ($1.14 < c < 1.1405$) one can hint a crisis of the very same kind.

Figure 10 corresponds to a zoom of the left and uppermost part of the bifurcation diagram in Figure 8. The Lyapunov exponent in the upper panel shows oscillations at band merging crises and, once again, a plateau (only visible in the inset) at the crisis located at $0.963 < c < 0.964$. An explanation for the occurrence of λ plateaus is deferred to Section 4.3.

For $c > 1$ and close to the critical point $b = 2$, the crises take place at integer values of ξ . This feature is illustrated in Figure 12. The left panel shows λ as a function of c for $b = 2.01$ and three different values of r . The right panel corresponds to the same data expressed in terms of ξ : All three curves collapse onto a master curve. Furthermore, the value of the Lyapunov exponent is invariant also in magnitude. This property fades as far as we move toward higher values of b , namely far from the critical point. All this buttresses the existence of universality in the system near the transition order-to-chaos.

Bifurcation diagrams of the VGH system always collapse when expressed in terms of z versus ξ . This is true even far from $b = 2$, in contrast with the Lyapunov exponent diagrams.

4.2. Far from $b = 2$

The lower panel of Figure 13 gives a view of the bifurcation diagram near $c = 1$, with $r = 4$ and $b = 2.1$, i.e. leaving the critical point. The upper panel shows an enlargement of the region located by the arrow below. This is again an instance of interior crisis. Concomitantly, the uppermost panel shows the variation of the Lyapunov exponent. At variance with Figures 8–10, here λ exhibits neither jumps nor plateaus across the window where the attractor shrinks. The reason is explained in the next subsection.

In the bifurcation diagram of Figure 14, with $b = 2.2$ and $r = 2$, the band merging phenomenon is more involved than in Figure 7. The corresponding Lyapunov exponent, in the upper panel, exhibits large variations at crises too. However, these do not take place any longer at integer values of ξ .

Eventually, in Figure 15, where $b = 3$, we observe that the Lyapunov exponent presents a large plateau whereas in the corresponding bifurcation diagram no interior crisis occurs. We have not found a justification for this case.

4.3. Interior crises and λ plateaus

An plausible explanation for the origin of λ plateaus occurring between interior crises pairs reads as follows. According to our numerical simulations, the narrow windows between interior crises of the VGH map resemble very much the so-called cycles of chaotic intervals, where the trajectories jump in a cyclic way from one chaotic band to another. Such a phenomenon occurs, for instance, in the logistic map [24] and is also termed in the literature as cyclic chaotic attractor or cyclic chaotic bands [25].

Trajectories look quite regular and, if the line $x_n = c$ in the bifurcation diagram does not cross any of the thin bands inside the window, then the proportion of exterior points ($x_n > c$) remains almost constant. As a consequence of it and taking into account the interpretation of λ for this map at the end of Section 2.3, the Lyapunov exponent gets the plateau shape. Otherwise, λ varies across the window, which is the case in Figure 13.

4.4. Crisis-induced intermittency

Next we gather some results, obtained from numerical simulations, concerning the behavior of trajectories around interior crises.

We commence by pointing out that interior crises in the VGH map appear in pairs. As the parameter c increases through a star value c_1^* the chaotic attractor suddenly shrinks into thin chaotic bands. This is the first interior crisis. Then, it exists a second star value $c_2^* > c_1^*$ where the set of thin bands suddenly widen and the attractor at $c > c_2^*$ recovers its old size. This is the second interior crisis of the pair. By contrast, in the logistic map, a tangent bifurcation precedes always an interior crises [12].

For values of c slightly different than a star value, in the region where the attractor widens ($c \lesssim c_1^*, c \gtrsim c_2^*$), the orbits spend long stretches in the region where the attractor is confined between the two crises. Occasionally, the trajectories burst and visit the whole attractor. This behavior, termed crisis-induced intermittency [12, 26], is illustrated in Figure 16. There, two orbits are plotted for slightly different values $c_1 = 0.8840$ and $c_2 = 0.8845$, located at both sides of the star value $c^* = 0.88411175\dots$. The empty square symbols stand for a trajectory in a regime where the attractor is still large. Intermittency is clearly observed. The solid dots represent a trajectory in a regime with shrunk attractor. It seems, at first glance, a period-8 orbit but the inset, which is a zoom of just one single narrow band, allows us to illustrate its non-periodic character.

For fixed c , the statistics of the length of stretches where the orbit stays confined in the region of the shrunk attractor is well described by an exponential distribution, provided $|c - c^*|$ is small, which yields a characteristic length $\tau(c)$. It has been shown [26] that for a large class of dynamical systems which exhibit crises, the dependence reads

$$\tau \sim |c - c^*|^{-\gamma}. \quad (23)$$

Indeed, this is the case for the VGH map. We have built up the statistics of τ as a function of $|c - c^*|$ for the case in Figure 16. The results are given in Figure 17. The linear fit in log-log scales yields a determination of the critical exponent: $\gamma = 0.89 \pm 0.02$.

4.5. A numerical flaw

Version (8) of the map presents a worth mentioning numerical nuisance. Namely, for some integer values of $b > 2$, computer generated trajectories collapse to an unstable periodic orbit after some iterations. A similar nature numerical artifact has been studied in [27, 28].

The dynamics for real z may be viewed as follows. For an initial point $z_0 < \xi$, every iteration conveys a shift to the right by two units until the condition $z_n > \xi$ is fulfilled. The second line in (8) may be read as: $\{(1 - b)\lfloor z_n \rfloor + 2\} + (1 - b)(z_n \bmod 1)$. Thus, for integer $b > 2$ the quantity in brackets is an integer and hence, its successive iteration conveys just a shift, as above. The key point is that, for finite machine precision, the last term dramatically loses precision in each iteration for some particular integer values of $b > 2$.

This effect may be understood on the basis of a generalization of the Bernoulli or binary shift map: $z_{n+1} = 2z_n \pmod{1}$. To this end, let us use the binary representation of the number $z_n \bmod 1$. Multiplication in base 2 is very simple in some cases. For instance, when $|1 - b| = 2^k$ we get the binary representation of the product $2^k(z_n \bmod 1)$ simply by shifting $k - 1$ places to the left every bit and (due to the finite precision of the computer) adding simultaneously $k - 1$ zeros to the right of the number. Henceforth this number gets shifted by two units in every iteration till it reaches $z_n > \xi$ when the mod operator acts again. This way, the piece in bracket is preserved as an integer under the action of the floor function, whereas the term $2^k(z_n \bmod 1)$ loses significant digits before going through the loop again. Eventually it stops when, after a number of iterations, $2^k(z_n \bmod 1) = 0$. At this point the iteration reduces to a periodic orbit with elements located at integer numbers. The full output is then a set of limit cycles whose elements are always integers. This misleading result is just consequence of the computer finite precision.

5. Discussion and conclusions

We have revisited a one-dimensional population model, proposed as an instance of density dependent dynamics. The fitness parameter b controls the onset of chaos. Values $b > 2$ convey chaos. Otherwise the system is regular. On the critical point $b = 2$ the attractor is made of an infinity of limit cycles that share a finite number of different periods. Hence, the transition order-to-chaos takes place through three steps: *i*) Finite number of limit cycles at $b < 2$; *ii*) Infinite number of limit cycles with finite number of different periods at $b = 2$; and *iii*) Chaos at $b > 2$. No period doubling occurs in this route to chaos. At $b = 2$, we have given an exact description of the system. We

have checked that such regular attractors have been sometimes plotted in bifurcation diagrams in the literature. However we have not found the concurrent descriptions of the attractor. Moreover, bifurcation diagrams may be found in the literature where this attractor lacks, most likely because too few initial seeds were used in the computation. An explanation for the phenomenon to occur has been provided on the basis of the power-law tail of the map.

The behavior of continuous piecewise linear maps has been studied in terms of the so-called border collision bifurcations. Thus, a thorough classification of the different kinds of bifurcations, in the parameter space, is given in [29]. The study explicitly excludes the borderline systems where a slope equals ± 1 . Interestingly, the VGH map in its version (8) with $\xi = 0$ ($c = 1$), falls just into this category. A study of discontinuous maps [30], namely with $\xi \neq 0$ (or $c \neq 1$), is flawed by the same restriction. Hence, the VGH map corresponds to a family of functions that are, by definition, out of those analyses. Moreover, in view of the results given in Section 3.2, this type of bifurcation may endow that classification with further structure.

An interesting phenomenon occurs close to the critical value, i.e. for $b \simeq 2$. There, the Lyapunov exponent of the VGH model exhibits renormalization features when expressed as a function of the variable ξ . In turn, the bifurcation diagrams as a function of c collapse for all r and b when expressed as $\{z_n, \xi\}$.

The abrupt variation of the Lyapunov exponent near band merging crises has already been reported [31]. Moreover, we have observed plateaus in the Lyapunov exponent, when represented as a function of c . It is worth mentioning that interior crises in the VGH map appear always in pairs.

We think that the the presence of a power-law piece in maps like the VGH model studied here originates worth knowing properties. We do hope that the variety of results gathered in this work may stimulate further work.

Acknowledgments. This work has been partially supported by contracts MCyT/FEDER, Spain (Grant No. FIS2004-0912) and Generalitat Valenciana, Spain (Grant No. ACOMP07/03). VBS thanks Generalitat Valenciana for financial support.

Appendix A. Exact piecewise linearization

Although by no means necessary, version (8) of the VGH dynamical system is extremely useful for analytic purposes and has a simple mathematical interpretation: it corresponds to two coupled affine dynamical systems. Precisely the new parameter ξ introduced acts as coupling constant.

For the general affine discrete dynamical system

$$x_{n+1} = Ax_n + B \tag{A.1}$$

the general solution with initial condition x_0 is

$$x_n = \begin{cases} x_0 + Bn, & \text{if } A = 1 \\ \left(x_0 + \frac{B}{A-1}\right) A^n - \frac{B}{A-1}, & \text{if } A \neq 1 \end{cases} \tag{A.2}$$

By itself system (A.1) has a rather dull dynamics. The evolution tends to the fixed point $B/(1 - A)$ if $|A| < 1$, whereas escapes to infinity if $|A| > 1$ or $A = 1$. For $A = -1$ any initial condition x_0 except the fixed point $B/2$ belongs to the 2-cycle $\{x_0, -x_0 + B\}$.

For the system (8), the coupling parameter ξ divides the phase space for our variable z in two regions: $z \leq \xi$ (Region I) and $z > \xi$ (Region II). In I (A.1) holds with $A = 1$, whereas $A = 1 - b < 0$ in region II. All over the phase space $B = 2$. The previous equation (A.2) is instrumental in discussing the transitions to and fro between both regions. These transitions explain the more complicated dynamics of the coupled system (8).

Transitions $I \rightarrow II$ from a point $z_0 \leq \xi$ will necessarily take place after N iterations with

$$N = \left\lfloor \frac{\xi - z_0}{2} \right\rfloor + 1 \quad (\text{A.3})$$

independently of the value of parameter b . Furthermore the orbit of $z_0 \leq \xi$ will land in II always with $z_N \in (\xi, \xi + 2]$.

In contrast, if $z_0 > \xi$ transitions $II \rightarrow I$ are not always possible and, when they actually occur, follow a more complicated pattern depending on b, ξ and z_0 . Concerning parameter b it is convenient to distinguish two possibilities:

$$\begin{aligned} A: & \quad 1 < b \leq 2 \\ B: & \quad b > 2. \end{aligned} \quad (\text{A.4})$$

As ξ and z_0 are concerned we set apart three cases:

$$\begin{aligned} \text{a:} & \quad \xi < z_0 \leq 0 \\ \text{b:} & \quad \xi \leq 0 < z_0 \\ \text{c:} & \quad 0 < \xi < z_0. \end{aligned} \quad (\text{A.5})$$

We have the following variants for case A in (A.4):

Aa: transitions $II \rightarrow I$ are forbidden.

Ab: transitions allowed only if $z_0 > (\xi - 2)/(1 - b)$ and then $N = 1$

Ac: transitions allowed for any z_0 if $\xi > 2/b$ or if $\xi < 2/b < z_0$ and $z_0 > (\xi - 2)/(1 - b)$.

In any case $N = 1$.

To discuss case B in (A.4) we introduce

$$\rho = \frac{\ln |(b\xi - 2)/(bz_0 - 2)|}{\ln(b - 1)}. \quad (\text{A.6})$$

We have the following variants:

Ba: transitions are always allowed and $N = 2\lceil \rho/2 \rceil$, in terms of the ceiling function.

Bb: If $z_0 < 2/b$ then $N = 2\lceil \rho/2 \rceil$. For $z_0 > 2/b$, if $z_0 < 4/b - \xi$ then $N = \lfloor \rho \rfloor + 1$ or $N = \lfloor \rho \rfloor + 2$ according to $\lfloor \rho \rfloor$ being even or odd. If $z_0 > 2/b$ and $z_0 > 4/b - \xi$ then $N = 1$.

Bc: the trajectory always crosses to region I with varying N according to the following scheme:

- (a) For $\xi < z_0 < 2/b$, $N = 2\lceil \rho/2 \rceil$
- (b) For $\xi < (2/b) < z_0 < (4/b - \xi)$, then $N = \lfloor \rho \rfloor + 1$ if $\lfloor \rho \rfloor$ is even, or $N = \lfloor \rho \rfloor + 2$ if $\lfloor \rho \rfloor$ is odd.
- (c) For $\xi < 2/b < 4/b - \xi < z_0$, $N = 1$
- (d) For $2/b < \xi$, $N = 1$, independently of $z_0 > \xi$

Appendix B. Detailed study of the system $b = 2$

Here we obtain the basins of attraction, periods, cycles and transients for the VGH map with $b = 2$ and arbitrary ξ and x_0 .

We analyze separately the cases $\xi < 0$ ($c < 1$), $\xi = 0$ ($c = 1$) and $\xi > 0$ ($c > 1$) with fixed $b = 2$. To facilitate the notation, in this Appendix we will use the z -version of the map, namely

$$z_{n+1} = \begin{cases} z_n + 2, & z_n \leq \xi \\ -z_n + 2, & z_n > \xi \end{cases} \quad (\text{B.1})$$

Appendix B.1. $\xi < 0$ (or $c < 1$)

The first general feature of the system is that the interval $[\xi, 2 - \xi]$ is invariant under the action of the map. This is readily appreciated on the bifurcation diagrams in figures 2 and 3. Every initial z_0 in the invariant interval belongs to a cycle of period two, with the exception $z_0 = 1$ which is a fixed point. The point $x_0 = 0$ (or equivalently $z_0 = -\infty$) is fixed $\forall c$ (respectively $\forall \xi$). The remaining points z_0 are eventually periodic and, after a transient, they enter the interval $[\xi, 2 - \xi]$. The z -phase space get partitioned as

$$(-\infty, \infty) = (-\infty, \xi] \cup (\xi, 2 - \xi) \cup [2 - \xi, \infty), \quad (\text{B.2})$$

which corresponds to the original x -phase space partition

$$(0, \infty) = (0, c] \cup (c, \frac{r}{c}) \cup [\frac{r}{c}, \infty). \quad (\text{B.3})$$

The dynamics of the map encompasses three cases, defined by the value of ξ :

- (i) $z_0 \leq \xi$ (or $x_0 \leq c$). Define $N \equiv \lfloor (\xi - z_0)/2 \rfloor$. Transient: $N + 1$. Limit cycle: $\{2(N + 1) + z_0, -2N - z_0\}$.
- (ii) $\xi < z_0 < 2 - \xi$ (or $c < x_0 < r/c$). No transient. Cycle: $\{z_0, 2 - z_0\}$. $z_0 = 1$ fixed point.
- (iii) $2 - \xi \geq z_0$ (or $r/c \geq x_0$). Define $N \equiv \lfloor (\xi + z_0)/2 \rfloor$. Transient: $N + 1$. Limit cycle: $\{2(N + 1) - z_0, -2N + z_0\}$.

Appendix B.2. $\xi = 0$ (or $c = 1$)

The invariant interval under the action of the map is $[0, 2]$, and their points belong to cycles of period two, with the exception $z_0 = 1$ which is a fixed point. Points $z_0 \notin [0, 2]$ are eventually periodic. The partition of the z -phase space is

$$(-\infty, \infty) = (-\infty, 0) \cup [0, 2] \cup (2, \infty), \quad (\text{B.4})$$

which corresponds to the original x -phase space partition

$$(0, \infty) = (0, 1) \bigcup [1, r] \bigcup (r, \infty). \quad (\text{B.5})$$

We distinguish four cases:

- (i) $z_0 < 0$ (or $x_0 < c = 1$). Define $N \equiv -\lfloor z_0/2 \rfloor$. Transient: N . Cycle: $\{2N + z_0, -2(N + 1) - z_0\}$.
- (ii) $z_0 = 0$ and $z_0 = 2$ constitute the cycle: $\{0, 2\}$.
- (iii) $0 < z_0 < 2$ with $z_0 \neq 1$. Cycle: $\{z_0, 2 - z_0\}$.
- (iv) $z_0 > 2$ (or $x_0 > r$). Define $N \equiv \lfloor z_0/2 \rfloor$. Transient: $N + 1$. Limit cycle: $\{2(N + 1) - z_0, z_0 - 2N\}$.

Appendix B.3. $\xi > 0$ (or $c > 1$)

This is the most involved situation. Here the invariant interval under the action of the map is $[-\xi, 2 + \xi]$. The remaining points are eventually periodic. The convenient partition of the z -phase space is

$$(-\infty, \infty) = (-\infty, -\xi) \bigcup [-\xi, 2 + \xi] \bigcup (2 + \xi, \infty). \quad (\text{B.6})$$

In the original x -phase space we have the partition

$$(0, \infty) = (0, \frac{1}{c}) \bigcup [\frac{1}{c}, rc] \bigcup (rc, \infty). \quad (\text{B.7})$$

Next we describe the features of the various intervals:

- (i) $z_0 < -\xi$ (or $x_0 < 1/c$). Transient: $\lfloor -(\xi + z_0)/2 \rfloor + 1$.
- (ii) $z_0 > 2 + \xi$ (or $x_0 > rc$). Transient: $\lfloor (z_0 - \xi)/2 \rfloor + 1$.
- (iii) $-\xi \leq z_0 \leq 2 + \xi$ (or $1/c \leq x_0 \leq rc$). This case embraces five possibilities according to the value of ξ :
 - (a) $0 < \xi < 1$. The convenient partition of the z -phase space is

$$\begin{aligned} [-\xi, 2 + \xi] &= \\ &[-\xi, 0) \bigcup [0, \xi] \bigcup (\xi, 2 - \xi) \\ &\bigcup [2 - \xi, 2) \bigcup [2, 2 + \xi] \\ &\equiv \mathcal{A} \bigcup \mathcal{B} \bigcup \mathcal{I} \bigcup \mathcal{C} \bigcup \mathcal{D}. \end{aligned} \quad (\text{B.8})$$

The subinterval $\mathcal{I} = (\xi, 2 - \xi)$ is, in turn, invariant under the action of the map. $z_0 = 1$ is a fixed point. Else, orbits are the period-2 cycles: $\{z_0, 2 - z_0\}$. The other four subintervals together form also an invariant subset. Their points hop in period-4 trajectories following the symbolic cyclic sequence: $\mathcal{A} \rightarrow \mathcal{C} \rightarrow \mathcal{B} \rightarrow \mathcal{D}$.

- (b) $\xi = 1$. The interval under scrutiny is now $(-1, 3)$. There exist the cycles: $\{-1, 1, 3\}$ and $\{0, 2\}$. Points $z_0 \neq -1, 0, 1, 2, 3$ are in cycles of period four.

(c) $1 < \xi < 2$. The convenient partition here reads:

$$\begin{aligned}
[-\xi, 2 + \xi] &= \\
[-\xi, \xi - 2] \cup (\xi - 2, 0) \cup \{0\} \\
\cup (0, 2 - \xi) \cup [2 - \xi, \xi] \cup (\xi, 2) \\
\cup \{2\} \cup (2, 4 - \xi) \cup [4 - \xi, 2 + \xi] \\
&\equiv \mathcal{A} \cup \mathcal{B} \cup \mathcal{C} \cup \mathcal{D} \cup \mathcal{E} \cup \mathcal{F} \cup \mathcal{G}.
\end{aligned} \tag{B.9}$$

There is no invariant subinterval under the map action. Four different types of periodic orbits exist. One period-2 trajectory which is the cycle $\{0, 2\}$. One period-3 trajectory which is the cycle $\{-1, 1, 3\}$. Period-4 orbits are, symbolically: $\mathcal{B} \rightarrow \mathcal{E} \rightarrow \mathcal{C} \rightarrow \mathcal{F}$, cyclic. Similarly, period-6 orbits follow the pattern:

$\mathcal{A} \rightarrow \mathcal{D} \rightarrow \mathcal{G} \rightarrow \mathcal{A} \rightarrow \mathcal{D} \rightarrow \mathcal{G}$, cyclic. Notice that every one of the three subintervals is visited twice in one cycle.

(d) $\xi = 2$. One period-3 cycle: $\{-1, 1, 3\}$. One period-4 cycle: $\{-2, 0, 2, 4\}$. The remaining orbits are period-6.

(e) $\xi > 2$. This is by far the most involved situation. We define the following quantities: $N \equiv \lfloor \xi/2 \rfloor$ and $\alpha \equiv \xi - 2N$. The convenient partition now depends on N and α :

$$\begin{aligned}
[-\xi, 2 + \xi] &= \\
J_N^- \cup H_{N-1}^- \cup J_{N-1}^- \cup \dots \cup H_0^- \\
\cup J_0^- \cup J_0^+ \cup H_0^+ \cup J_1^+ \cup H_1^+ \\
\cup \dots \cup J_N^+ \cup H_N^+ \cup J_{N+1}^+ \\
\cup \mathcal{A} \cup \mathcal{B} \cup \mathcal{C} \cup \mathcal{D}.
\end{aligned} \tag{B.10}$$

The length of the subintervals J 's and H 's is α and $2 - \alpha$ respectively. The super-index tells whether the interval is located either to the left ($-$) or to the right ($+$) of $z = 0$. The sub-index codes the borders location of the interval according to

$$\begin{aligned}
J_k^+ &= (2k, 2k + \alpha), \\
H_k^+ &= (2k + \alpha, 2(k + 1)), \\
J_k^- &= (-2k - \alpha, -2k), \\
H_k^- &= (-2(k + 1), -2k - \alpha).
\end{aligned}$$

Besides

$$\begin{aligned}
\mathcal{A} &= \{2k + \alpha; k = 0 \dots N + 1\}, \\
\mathcal{B} &= \{-2k - \alpha; k = 0 \dots N\}, \\
\mathcal{C} &= \{2k; k = -N \dots N + 1\}, \\
\mathcal{D} &= \{2k + 1; k = -N \dots N\}.
\end{aligned}$$

Table B1. Period of the trajectories according to the initial point $z_0 \in [-\xi, 2 + \xi]$, with $b = 2$ and $\xi > 2$, in equation (8).

| Initial point | η | Period | Condition |
|--|--------------------|----------|---------------------|
| $z_0 \in J_k^\pm$ and $\notin \mathcal{D}$ | $-2k \pm z_0$ | $4N + 6$ | $\eta + \alpha > 2$ |
| | | $4N + 4$ | $\eta + \alpha < 2$ |
| $z_0 \in H_k^\pm$ and $\notin \mathcal{D}$ | $2(k + 1) \mp z_0$ | $4N + 2$ | $\eta > \alpha$ |
| | | $4N + 4$ | $\eta < \alpha$ |
| $z_0 \in \mathcal{A} \cup \mathcal{B}$ | | $4N + 6$ | $\alpha > 1$ |
| | | $4N + 4$ | $\alpha < 1$ |
| $z_0 \in \mathcal{D}$ | | $2N + 3$ | $\alpha > 1$ |
| | | $2N + 1$ | $\alpha < 1$ |
| $z_0 \in \mathcal{C}$ | | $2N + 2$ | $\forall \alpha$ |

The period of any trajectory starting in $[-\xi, 2 + \xi]$ is given in Table B1, where we have defined an auxiliary quantity η when appropriate.

- [1] May R M 1976 Simple mathematical-models with very complicated dynamics *Nature* **261** 459–67
- [2] May R M, Conway G R, Hassell M P and Southwood T R E 1974 Time delays, density-dependence and single-species oscillations *J. Anim. Ecol.* **43** 747–70
- [3] Hassell M P 1975 Density-dependence in single-species populations *J. Anim. Ecol.* **44** 283–95
- [4] Varley G C, Gradwell G R and Hassell M P 1973 *Insect population ecology: an analytical approach* (Oxford: Blackwell)
- [5] May R M and Oster G F 1976 Bifurcations and dynamic complexity in simple ecological models *Am. Nat.* **110** 573–99
- [6] May R M 1975 Biological populations obeying difference equations: Stable points, stable cycles, and chaos *J. theor. Biol.* **51** 511–24
- [7] Banerjee S and Verghese G C 2001 *Nonlinear phenomena in power electronics: Attractors, bifurcations, chaos and nonlinear control* (New York: IEEE Press)
- [8] Hogan S J, Higham L and Griffin T C L 2007 Dynamics of a piecewise linear map with a gap *Proc. R. Soc. A* **463** 49–65
- [9] Hilborn R C 2000 *Chaos and nonlinear dynamics* (Oxford University Press)
- [10] Strogatz S H 1994 *Nonlinear Dynamics and Chaos* (Cambridge MA: Perseus Books)
- [11] Collet P and Eckmann J P 1980 *Iterated Maps on the Interval as Dynamical Systems* (Birkhäuser)
- [12] Ott E 2002 *Chaos in dynamical systems* (Cambridge University Press)
- [13] Oteo J A and Ros J 2007 Double precision errors in the logistic map: Statistical study and dynamical interpretation *Phys. Rev. E* **76** 036214–22
- [14] Bailey D H 1993 Algorithm 719: Multiprecision translation and execution of Fortran programs *ACM Trans. Math. Software* **19** 288–319
- [15] Bailey D H 2005 High-precision floating-point arithmetic in scientific computation *Comput. Sci. Eng.* **7** 54–61
- [16] Costa U M S, Lyra M L, Plastino A R and Tsallis C 1997 Power-law sensitivity to initial conditions within a logisticlike family of maps: Fractality and nonextensivity *Phys. Rev. E* **56** 245–50
- [17] Tsallis C, Plastino A R and Zheng W M Power-law sensitivity to initial conditions: New entropic representation 1997 *Chaos, Solitons & Fractals* **8** 885–91

- [18] Grebogi C, Ott E and Yorke J A 1983 Crises, sudden changes in chaotic attractors, and transient chaos *Physica D* **7** 181–200
- [19] Jensen R V and Myers C R 1985 Images of the critical points of nonlinear maps *Phys. Rev. A* **32** 1222–4
- [20] Eidson J, Flynn S, Holm C, Weeks D and Fox R F 1986 Elementary explanation of boundary shading in chaotic-attractor plots for the Feigenbaum map and the circle map *Phys. Rev. A* **33** 2809–12
- [21] Feigenbaum M J 1978 Quantitative universality for a class of non-linear transformations *J. Stat. Phys.* **19** 25–52
- [22] Feigenbaum M J 1979 Universal metric properties of non-linear transformations *J. Stat. Phys.* **21** 669–706
- [23] Lai Y C, Grebogi C and Yorke J A 1992 Sudden change in the size of chaotic attractors: How does it occur? *Applied Chaos* (chapter 19) Ed. by Kim H and Stringer J (John Wiley & Sons, Inc.)
- [24] Beck C and Schlögl F 1993 *Thermodynamics of chaotic systems* (Cambridge University Press)
- [25] Maistrenko Yu L, Maistrenko V L and Chua L O 1993 Cycles in chaotic intervals in a time-delayed Chua's circuit *Int. J. Bifurcation and Chaos* **3** 1557–72
- [26] Grebogi C, Ott E, Romeiras F and Yorke J A 1987 Critical exponents for crisis-induced intermittency *Phys Rev E* **36** 5365–79
- [27] Diamond P, Kloeden P, Pokrovskii A and Vladimirov A 1995 Collapsing effects in numerical simulations of a class of chaotic dynamical systems and random mappings with a single attracting center *Physica D* **86** 559–71
- [28] Yuan G and Yorke J A 2000 Collapsing of chaos in one dimensional maps *Physica D* **136** 18–30
- [29] Banerjee S, Karthik M S, Yuan G and Yorke J A 2000 Bifurcations in one-dimensional piecewise smooth maps: Theory and applications in switching circuits *IEEE Trans. Circuits Syst.-I: Fund. Theory Appl.* **47** 389–94
- [30] Avrutin V and Schanz M 2006 On multi-parametric bifurcations in a scalar piecewise linear map *Nonlinearity* **19** 531–52
- [31] Mehra V and Ramaswamy R 1996 Maximal Lyapunov exponent at crises *Phys. Rev. E* **53** 3420–4

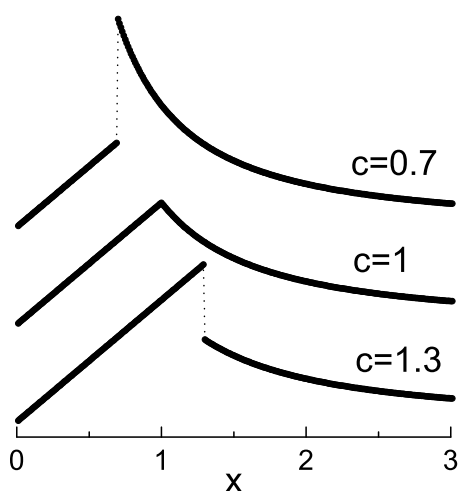


Figure 1. Shape of the map (5) for $b = 2.5$, $r = 2$ and three different values $c = 0.7, 1, 1.3$. The curves have been vertically shifted for the sake of clarity.

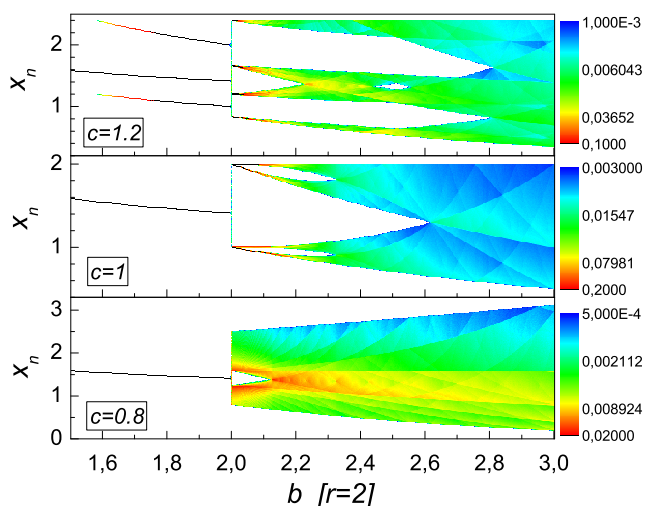


Figure 2. (Color online) Bifurcation diagrams as a function of b , for $r = 2$ and three different values of c . The color scale is logarithmic and it stands for the frequency the point is visited with. This holds for the rest of color figures, unless otherwise stated.

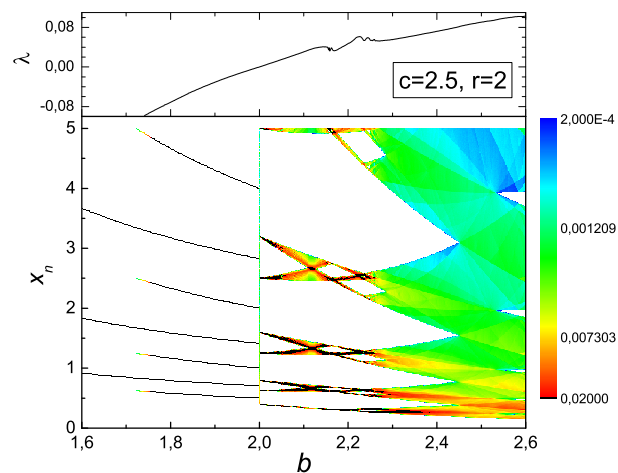


Figure 3. (Color online) Bifurcation diagram as a function of b , for $r = 2$, $c = 2.5$. The corresponding Lyapunov exponent is in the upper panel.

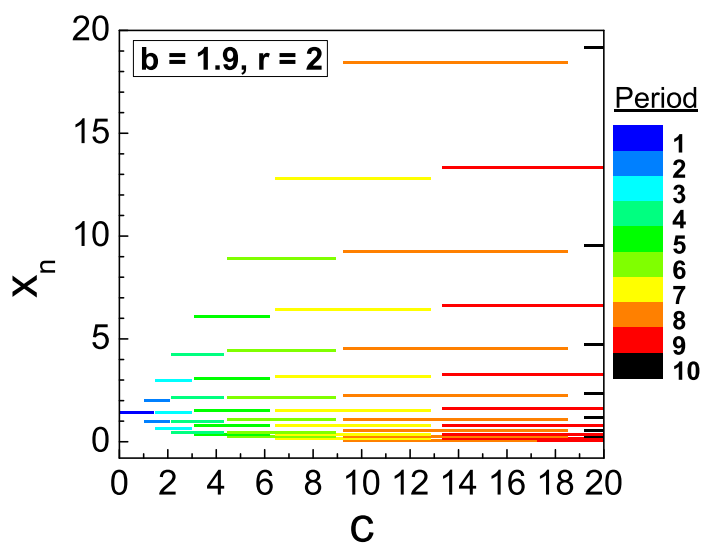


Figure 4. (Color online) Regular orbits. Bifurcation diagram as a function of c , with $b = 1.9$ and $r = 2$. The period of cycles is coded by the color scale (gray tone).

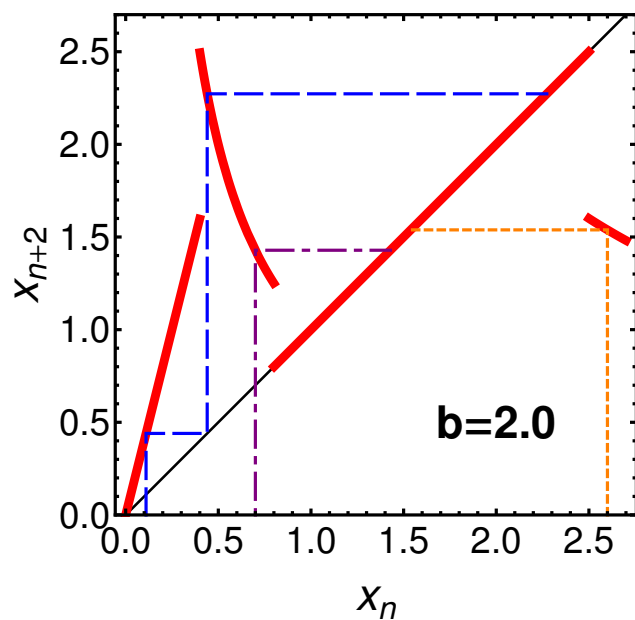


Figure 5. (Color online) Cobweb plot for $f^{[2]}$ (thick red line). Parameter values: $b = r = 2, c = 0.8$. The three seeds are $x_0 = 0.11, 0.7, 2.6$, and are eventually stable fixed points of $f^{[2]}$.

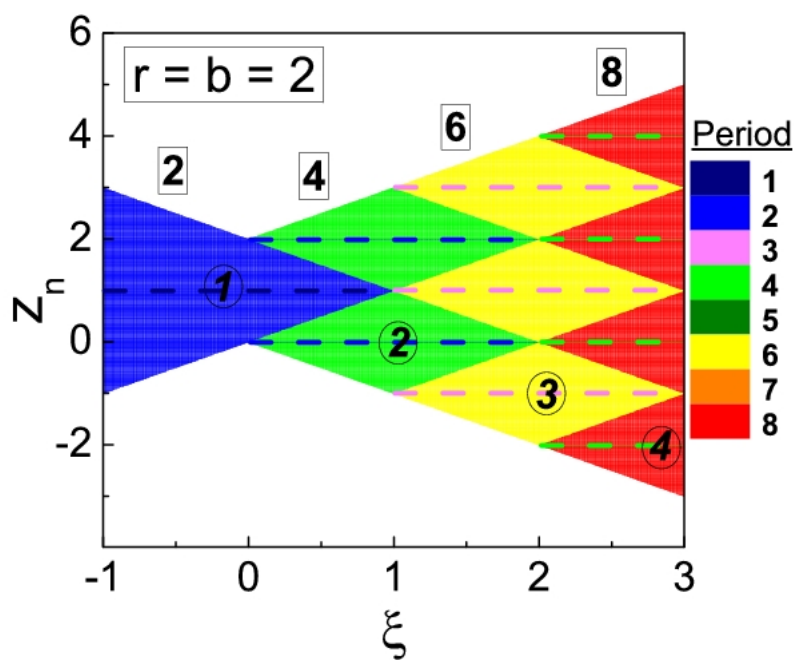


Figure 6. (Color online) Bifurcation diagram for $r = b = 2$. The color (gray tone) codes the period of the cycle which is also given by the framed numbers for trajectories falling in rhombuses. The circled numbers stand for the periods of the cycles falling on dashed lines.

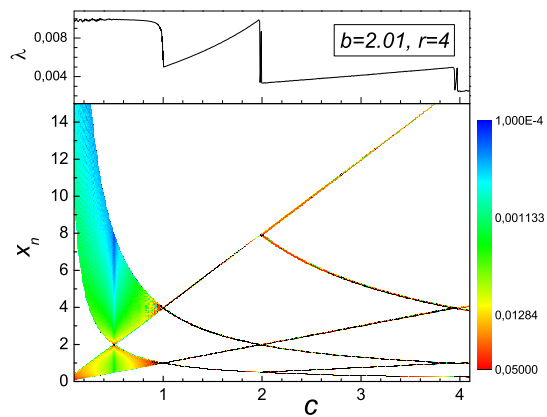


Figure 7. (Color online) Bifurcation diagram (bottom panel) and Lyapunov exponent (upper panel) obtained using $b = 2.01$ and $r = 4$.

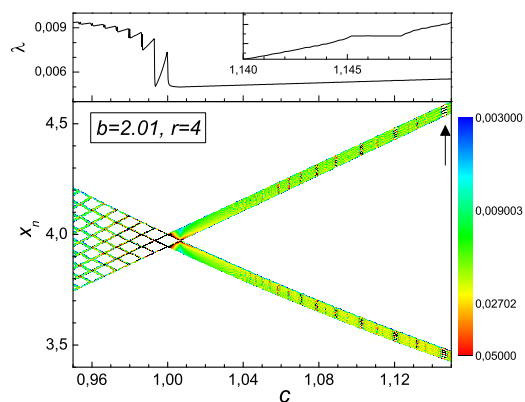


Figure 8. (Color online) Bifurcation diagram (bottom panel) and Lyapunov exponent (upper panel) obtained using $b = 2.01$ and $r = 4$. This plot presents a zoom of Figure 7. The inset in the upper panel allows to appreciate the plateau in λ .

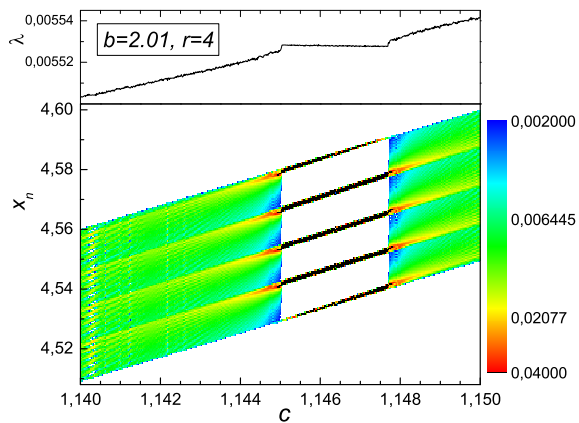


Figure 9. (Color online) Bifurcation diagram (bottom panel) and Lyapunov exponent (upper panel) obtained using $b = 2.01$ and $r = 4$. This plot presents a zoom of Figure 8 in the region located by the arrow. It exhibits interior crises.

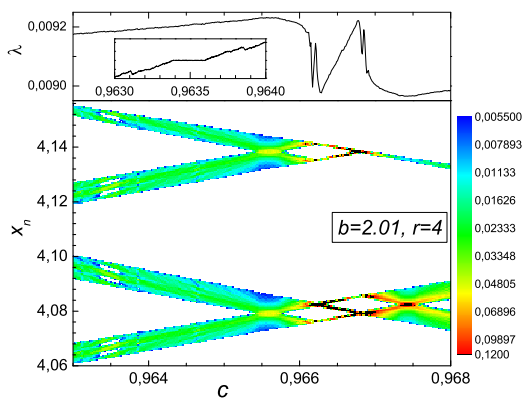


Figure 10. (Color online) Bifurcation diagram (bottom panel) and Lyapunov exponent (upper panel) obtained using $b = 2.01$ and $r = 4$. This plot presents a zoom of Figure 8. The inset in the upper panel allows to appreciate the plateau in λ .

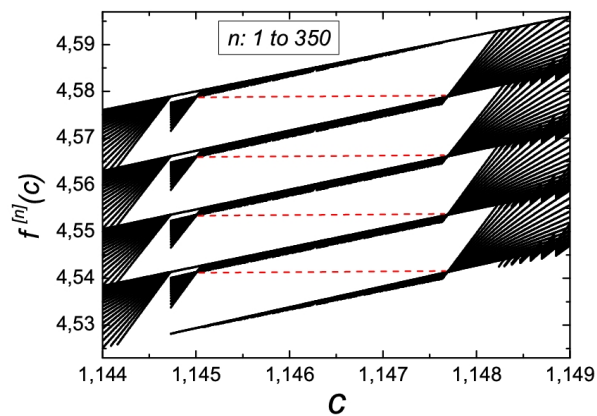


Figure 11. (Color online) Detail of the first 350 Harter curves obtained using $b = 2.01$ and $r = 4$. Dashed (red) lines between crossings of harter curves correspond to unstable fixed points.

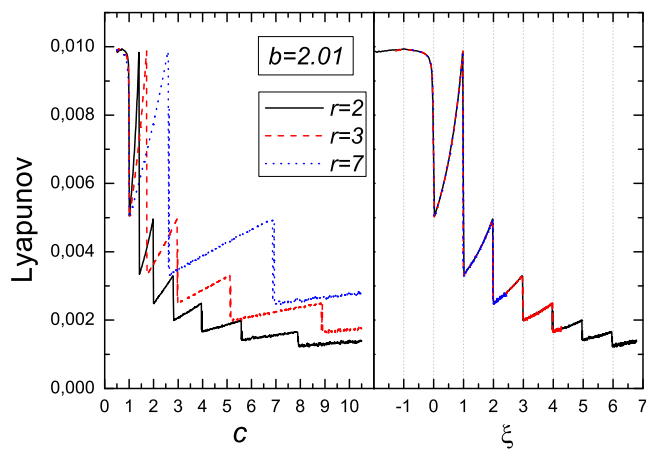


Figure 12. (Color online) Left panel: Lyapunov exponent as a function of c for three values of r . Right panel: Collapse of the same three curves as a function of ξ

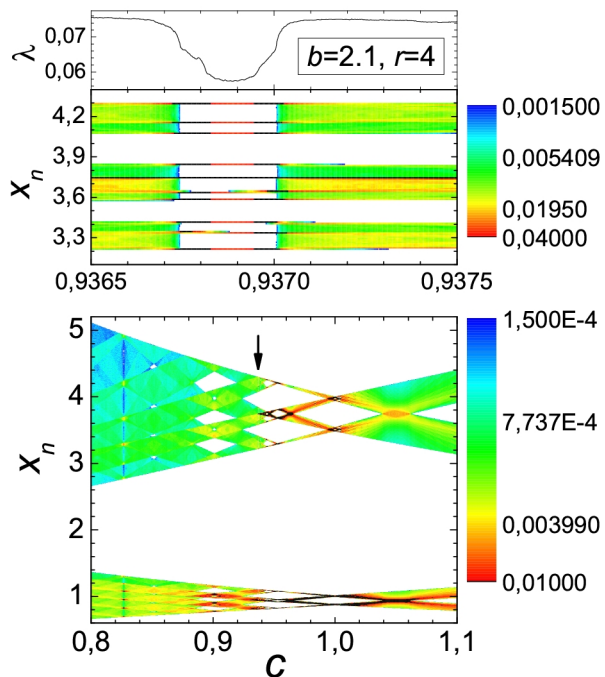


Figure 13. (Color online) Bottom panel: Bifurcation diagram as a function of c , with $b = 2.1$ and $r = 4$. The arrow locates the narrow window zoomed in the upper panel where λ is also shown.

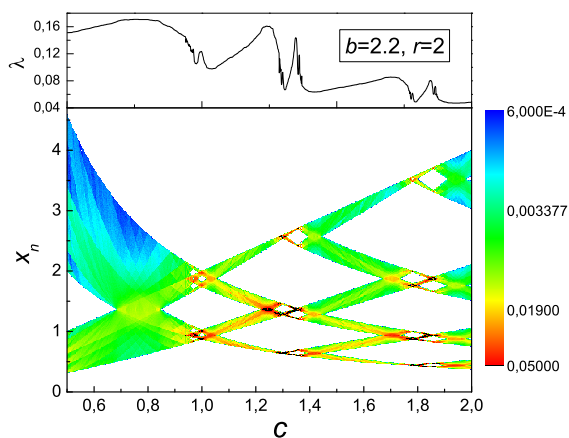


Figure 14. (Color online) Bifurcation diagram and Lyapunov exponent as a function of c . This particular plot was obtained using $b = 2.2$ and $r = 2$. The system is not close to the critical point $b = 2$.

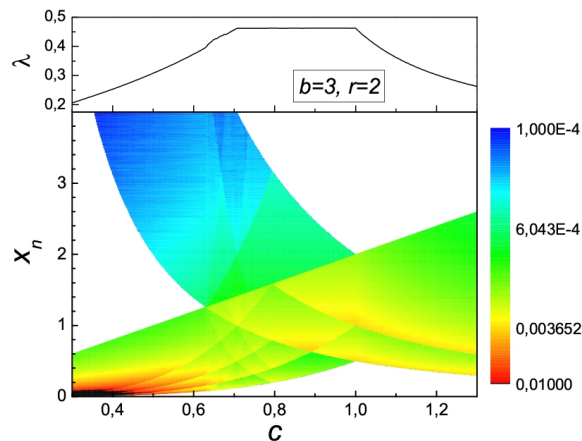


Figure 15. (Color online) Bifurcation diagram and Lyapunov exponent as a function of c , with $b = 3$ and $r = 2$.

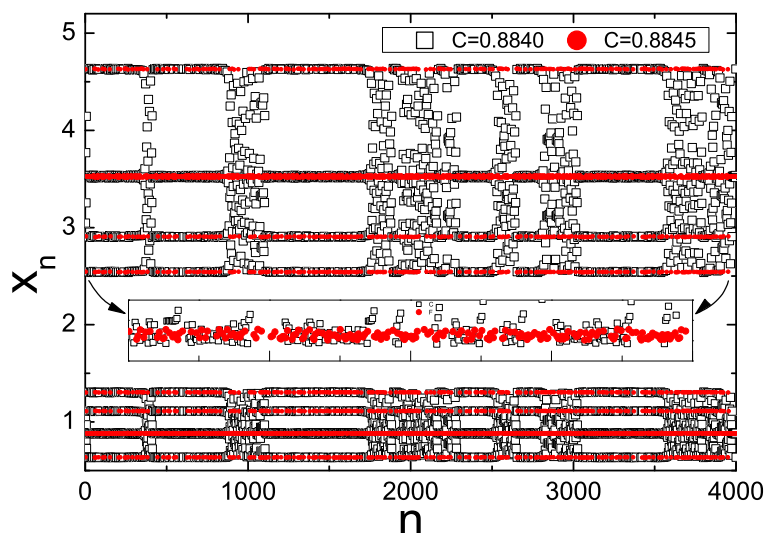


Figure 16. (Color online) Crisis-induced intermittency, with $r = 4$ and $b = 2.2$. Two trajectories from both sides of the critical value $c^* = 0.88411175\dots$ are compared. Solid dots (red) correspond to a trajectory with $c = 0.8845$, where the attractor splits in narrow bands. Empty squares (black) correspond to $c = 0.8840$, namely in the wider region of the attractor. The inset is a zoom of the points close to $x = 2.5$ and allows to illustrate the non-regular character of these trajectories.

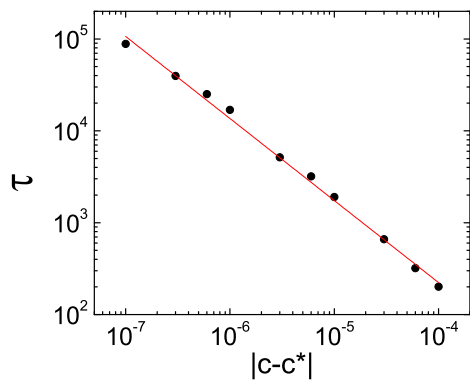


Figure 17. (Color online) Characteristic length τ versus $|c - c^*|$ in log-log scales. Each dot was obtained from 100 initial conditions and series of 10^6 iterates, with $c^* = 0.88411175$, $b = 2.2$ and $r = 4$. The slope of the linear fit is $\gamma = -0.89 \pm 0.02$.